Electrostatic Potential Distribution through a Rectangular Aperture in a Thick Conducting Plane

Hyun H. Park and Hyo J. Eom

***Abstract*—A potential distribution through a rectangular aperture in a thick conducting plane is examined when the incident electric field is normal to the rectangular aperture. The Fourier-transform is used to represent the potential in the spectral domain and the boundary conditions are enforced to represent a solution in closed form. Numerical computations are performed to illustrate the behavior of the potential distribution through a thick rectangular aperture. Our solution for the electric polarizability is represented in rapidly converging series so that it is numerically efficient.**

I. Introduction

An electrostatic potential distribution through various aperture shape in a conducting plane has been of considerable interest in the area of microwaves [1], [2]. A potential distribution through a rectangular aperture in a thin conducting plane is studied in [2] using a variational technique. A potential distribution through an infinitely long slit in a thick conducting plane is re-examined in [3] using the Fourier-transform and the mode-matching technique. In this paper we investigate a problem of the potential distribution through a rectangular aperture in a thick conducting plane by extending the technique used in [3]. Our Fourier-transform technique is novel in that it allows us to obtain a solution without a recourse to the conventional Schwarz–Christoffel transformation. In the next section, we derive a rapidly converging series solution for the electric polarizability which is numerically very efficient.

II. Field Analysis

Consider a rectangular aperture in a perfectly-conducting thick plane at zero potential. In region (I) ($z > 0$), an incident potential Φ^i impinges on a rectangular aperture. We wish to find an electrostatic potential distribution through the rectangular aperture. In region (I) the potential consists of the incident and scattered potentials as

$$\Phi^i(x,y,z) = z \tag{1}$$

$$\Phi^s(x,y,z) = \frac{1}{(2\pi)^2}\int_{-\infty}^{\infty}\int_{-\infty}^{\infty}\tilde{\Phi}^s(\zeta,\eta) \cdot \exp(-i\zeta x - i\eta y - \sqrt{\zeta^2+\eta^2}z)\; d\zeta\; d\eta. \tag{2}$$

In region (II) ($-d < z < 0, |x| < a, |y| < b$) the total potential is

$$\Phi^d(x,y,z) = \sum_{m=1}^{\infty}\sum_{n=1}^{\infty}[c_{mn}\sinh k_{mn}(z+d) + d_{mn} \cdot \cosh k_{mn}(z+d)] \times \sin a_m(x+a) \cdot \sin b_n(y+b) \tag{3}$$

where

$$a_m = \frac{m\pi}{2a}, \quad b_n = \frac{n\pi}{2b}, \quad \text{and} \quad k_{mn} = \sqrt{a_m^2 + b_n^2}.$$

Manuscript received November 11, 1995; revised June 14, 1996.

The authors are with the Department of Electrical Engineering, Korea Advanced Institute of Science and Technology, 373-1, Kusong Dong, Yusung Gu, Taejon, Korea.

Publisher Item Identifier S 0018-9480(96)06914-1.

In region (III) ($z < -d$) the transmitted potential is

$$\Phi^t(x,y,z) = \frac{1}{(2\pi)^2}\int_{-\infty}^{\infty}\int_{-\infty}^{\infty}\tilde{\Phi}^t(\zeta,\eta) \cdot \exp[-i\zeta x - i\eta y + \sqrt{\zeta^2+\eta^2}(z+d)]\; d\zeta\; d\eta. \tag{4}$$

To determine the unknown coefficients c_{mn} and d_{mn}, we enforce the boundary condition on the field continuities.

First

$$\Phi^i(x,y,0) + \Phi^s(x,y,0) = \begin{cases} \Phi^d(x,y,0) & \text{for } |x| < a, |y| < b \\ 0 & \text{otherwise.} \end{cases} \tag{5}$$

Applying the Fourier-transform

$$\int_{-\infty}^{\infty}\int_{-\infty}^{\infty}(5)e^{i\zeta x + i\eta y}\; dx\; dy$$

we obtain

$$\tilde{\Phi}^s(\zeta,\eta) = \sum_{m=1}^{\infty}\sum_{n=1}^{\infty}[c_{mn}\sinh(k_{mn}d) + d_{mn}\cosh(k_{mn}d)] \cdot a_m b_n (ab)^2 F_m(\zeta a) F_n(\eta b) \tag{6}$$

where

$$F_m(u) = \frac{(-1)^m e^{iu} - e^{-iu}}{(u)^2 - \left(\frac{m\pi}{2}\right)^2}. \tag{7}$$

Second

$$\left.\frac{\partial[\Phi^i(x,y,z) + \Phi^s(x,y,z)]}{\partial z}\right|_{z=0} = \left.\frac{\partial\Phi^d(x,y,z)}{\partial z}\right|_{z=0} \quad \text{for} \quad |x| < a, |y| < b. \tag{8}$$

Rewriting (8) for $|x| < a, |y| < b$,

$$1 - \frac{1}{(2\pi)^2}\int_{-\infty}^{\infty}\int_{-\infty}^{\infty}\sqrt{\zeta^2+\eta^2}\tilde{\Phi}^s(\zeta,\eta)e^{-i\zeta x - i\eta y}\; d\zeta\; d\eta = \sum_{m=1}^{\infty}\sum_{n=1}^{\infty}k_{mn}[c_{mn}\cosh(k_{mn}d) + d_{mn}\sinh(k_{mn}d)] \cdot \sin a_m(x+a)\sin b_n(y+b). \tag{9}$$

Substituting (6) into (9), multiplying (9) by $\sin a_p(x+a)\sin b_q(y+b)\; dx\; dy$ ($p, q = 1, 2, 3, \cdots$), and performing integration

$$\gamma_{pq} - \frac{a_p b_q}{(2\pi)^2}(ab)^3\sum_{m=1}^{\infty}\sum_{n=1}^{\infty}a_m b_n \cdot [c_{mn}\sinh(k_{mn}d) + d_{mn}\cosh(k_{mn}d)]I_{mnpq} = k_{pq}[c_{pq}\cosh(k_{pq}d) + d_{pq}\sinh(k_{pq}d)] \tag{10}$$

where

$$\gamma_{pq} = \frac{4[1-(-1)^p][1-(-1)^q]}{pq\pi^2} \tag{11}$$

$$I_{mnpq} = \int_{-\infty}^{\infty}\int_{-\infty}^{\infty}\sqrt{\zeta^2+\eta^2}F_m(\zeta a)F_p(-\zeta a) \cdot F_n(\eta b)F_q(-\eta b)\; d\zeta\; d\eta. \tag{12}$$

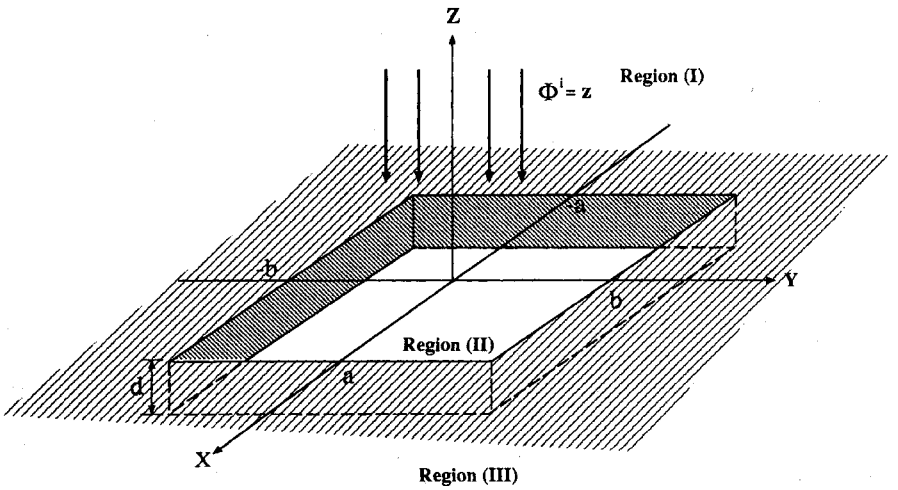

Fig. 1. Geometry of a rectangular aperture in a thick conducting plane.

TABLE I
CONVERGENCE RATE OF SERIES c_{mn} AND d_{mn} ($d/a = 0.5, c_{mn} = d_{mn} = 0$ FOR $m, n = 2, 4, 6, \cdots$)

m	c_{mn}	d_{mn}	$\Phi^d(0,0,0)$	$\Phi^d(0,0,-d)$
1	0.243587	0.289937	0.817658	0.289932
3	0.000362	0.001913	0.608610	0.258101
5	-0.000164	0.000220	0.649437	0.262396
7	-0.000079	0.000081	0.621178	0.259759
9	-0.000043	0.000043	0.638491	0.261645
11	-0.000027	0.000027	0.624793	0.260036

The numerical evaluation of I_{mnpq} is efficient in that it decays as $1/\zeta^2$ when $\zeta \to \pm\infty$. Similarly from the boundary conditions at $z = -d$, we get

$$\frac{a_p b_q}{(2\pi)^2}(ab)^3 \sum_{m=1}^{\infty}\sum_{n=1}^{\infty} a_m b_n d_{mn} I_{mnpq} = k_{pq} c_{pq} \tag{13}$$

From (10) and (13) we obtain the matrix equation for c_{mn} and d_{mn}

$$\begin{bmatrix} \Psi_1 & \Psi_2 \\ \Psi_3 & \Psi_4 \end{bmatrix} \begin{bmatrix} C \\ D \end{bmatrix} = \begin{bmatrix} \Gamma \\ 0 \end{bmatrix} \tag{14}$$

where C, D, and Γ are column vectors of c_{mn}, d_{mn}, and γ_{pq},

$$\psi_{1,mnpq} = k_{pq}\cosh(k_{pq}d)\delta_{mp}\delta_{nq} + \frac{a_p b_q}{4\pi^2}(ab)^3 a_m b_n I_{mnpq}\sinh(k_{mn}d) \tag{15}$$

$$\psi_{2,mnpq} = k_{pq}\sinh(k_{pq}d)\delta_{mp}\delta_{nq} + \frac{a_p b_q}{4\pi^2}(ab)^3 a_m b_n I_{mnpq}\cosh(k_{mn}d) \tag{16}$$

$$\psi_{3,mnpq} = -k_{pq}\delta_{mp}\delta_{nq} \tag{17}$$

$$\psi_{4,mnpq} = \frac{a_p b_q}{4\pi^2}(ab)^3 a_m b_n I_{mnpq} \tag{18}$$

and δ_{mp} is the Kronecker delta. When $d \to \infty$, the solution is

$$C = (\Psi_1 + \Psi_2)^{-1}\Gamma \tag{19}$$

$$D = -C. \tag{20}$$

When region (III) is filled with a perfect conductor at zero potential,

$$D = \Psi_2^{-1}\Gamma \tag{21}$$

$$C = 0. \tag{22}$$

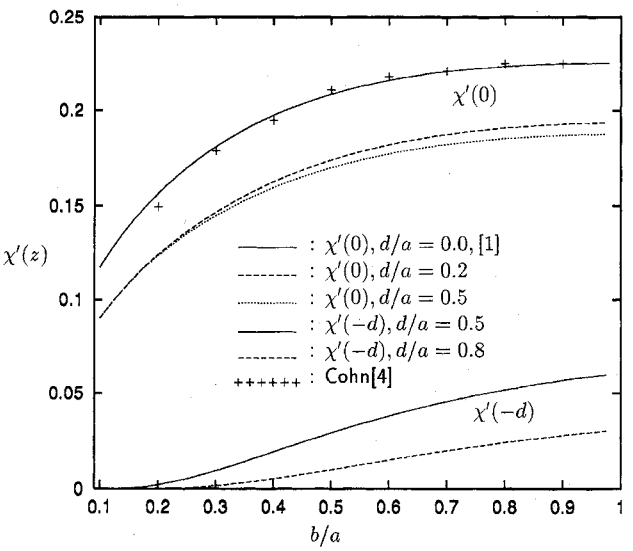

Fig. 2. Behavior of the normalized polariability $\chi'(z)$ versus b/a.

The electric polarizability defined in [2] is

$$\chi(z) \equiv 2\int_{-b}^{b}\int_{-a}^{a} \Phi^d(x,y,z)\,dx\,dy = 2ab\sum_{m=1}^{\infty}\sum_{n=1}^{\infty}\gamma_{mn}[c_{mn}\sinh k_{mn}(z+d) + d_{mn}\cdot\cosh k_{mn}(z+d)]. \tag{23}$$

Fig. 2 shows the normalized electric polarizability $\chi'(z) \equiv \chi(z)/(4ab)^{1.5}$ versus b/a for different d/a, illustrating our results agree well with experimental data [4] when $d/a = 0$. We also confirm that our curve for $d/a = 0$ agrees perfectly with the polynomial solution in [1]. We note that when $d/a > 0.5, \chi'(0)$ remains almost insensitive to a change in d/a. Table I shows a convergence rate of the series c_{mn} and d_{mn} when $d/a = 0.5$. Our computational experience shows that a use of the first four terms ($m = 1, 3, 5, 7$) gives accurate results with less than 2% error. A typical CPU time to evaluate c_{mn} and d_{mn} is less than one minute on a SPARC-20 Workstation. This means that our series solution is rapidly-converging and numerically efficient.

III. Conclusion

The potential distribution through a thick conducting rectangular aperture is studied using the Fourier-transform and the mode-matching technique. The normalized electric polarizability is insensitive to a change in d/a when $d/a > 0.5$. The solution is represented in rapidly-convergent series form which is numerically very efficient.

References

[1] N. A. McDonald, "Polynomial approximations for the electric polarizabilities of some small apertures," *IEEE Trans. Microwave Theory Tech.*, vol. 33, no. 11, pp. 1146–1149, Nov. 1985.

[2] R. L. Gluckstern and R. K. Cooper, "Electric polarizability and magnetic susceptibility of small holes in a thin screen," *IEEE Trans. Microwave Theory Tech.*, vol. 38, no. 2, pp. 186–192, Feb. 1990.

[3] Y. S. Kim and H. J. Eom, "Fourier-transform analysis of electrostatic potential distribution through a thick slit," *IEEE Trans. Electromag. Compat.*, vol. 38, no. 1, pp. 77–79, Feb. 1996.

[4] S. B. Cohn, "The electric polarizability of aperture of arbitrary shape," *Proc. I.R.E.*, vol. 40, pp. 1069–1071, 1952.

Photovoltaic-FET for Optoelectronic RF/μwave Switching

C. K. Sun, R. Nguyen, C. T. Chang, and D. J. Albares

Abstract—**A photovoltaic-FET (PV-FET) is demonstrated for RF/μwave switching with performance improved over other optoelectronic switches reported while operating with 10-100 times less optical power. The PV-FET characteristics were 3 Ω on-resistance, > 30 MΩ off-resistance under <1 mW optical power, and 300 fF switch capacitance. This PV-FET was inductor tuned at 790 MHz and 7.4 GHz to enhance isolation, intended for reconfigurable antenna applications. The measured insertion loss and isolation agree well with those from theoretical calculation and numerical circuit simulation based on the switch parameters. The measured switch rise and fall times were 20 μs and 2 μs, respectively. Controlled by light via optical fiber, the PV-FET can be used for remote RF/μwave switching control with no electrical bias, complete electromagnetic, and good thermal isolation.**

I. Introduction

Optically activated electronic switches or optoelectronic (OE) switches have long been investigated for generating and sampling ultrafast electrical pulses [1]–[3]. Recently, OE switches controlled by light via optical fibers and without electrical bias have been considered for RF/μwave (abbreviated RF hereafter) switching due to unique and often decisive advantages of the electromagnetically and thermally isolated control lines. Other appealing features offered by optical fibers are small size, lightweight, and low loss (long distances). Potential applications of such an OE switch include reconfigurable antennas [4], programmable antenna feeds and tuned networks, and switching within cryogenic electronic circuits [5]. The OE switch configuration and characteristics required in each application vary. Typical OE switches for reconfigurable antennas are used in series connection between antenna segments. The required characteristics are low on-resistance R_{on} (<5 Ω), high off-resistance R_{off} (>10 kΩ), low capacitance C (<300 fF, for C to X band), bias-free operation, and low optical control power. Needed switching speeds range from ms to ns and power handling ranges from μW to hundreds of watts.

Manuscript received November 6, 1995; revised June 14, 1996.

The authors are with NCCOSC RDT&E Div., San Diego, CA 92152-5000 USA.

C. T. Chang is with the Department of Electrical and Computer Engineering, San Diego State University, San Diego, CA 92182 USA.

Publisher Item Identifier S 0018-9480(96)06915-3.

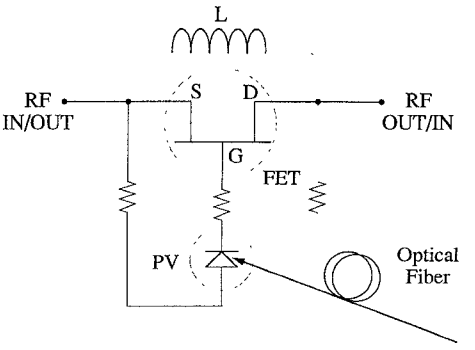

Fig. 1. Circuit schematic of the PV-FET switch with a depletion-mode FET. An inductor L in parallel with the FET may be used to enhance the isolation at the vicinity of the tuned frequency. Without the tuning inductor, a resistor between the gate and drain is used for electrical bias.

OE switches such as photoconductor [6], [7], surface-depleted optical FET [8], [9], and direct optically illuminated FET [10] have been investigated, but they lacked the switch characteristics mentioned above and generally required high optical power. A photoconductive switch under high optical power (>50 mW) obtained low R_{on} of 2 Ω, but suffered from low R_{off} ($\leq$1 kΩ) and millisecond switching time. The surface-depleted optical FET was activated by low optical power ($\sim$1 mW) but had low RF power handling capability ($\sim$1 mW). The direct optical illuminated FET can be used as an optically controlled switch but requires external electrical gate biasing (via metal wire) which compromises electromagnetic and thermal isolation.

A photovoltaic-FET (PV-FET) switch has been reported with R_{on} of 65 Ω and C of 65 fF [9]. We report a PV-FET with improved performance and the introduction of tuning to enhance isolation as a series switch for reconfigurable antennas [4], [9]. We obtain $R_{on} \approx 3\ \Omega$, $R_{off} > 30$ MΩ under <1 mW optical power, and $C \approx 300$ fF. These parameters are consistent with the measured insertion loss of 0.33 dB and the untuned isolation of 17 dB at 790 MHz. Tuning out the FET capacitance at 790 MHz gives an isolation of 57 dB and tuning at 7.4 GHz gives 23 dB isolation. The switching speed of the tuned PV-FET at 790 MHz is measured to be 20 μs rise time and 2 μs fall time. The power handling capability is estimated to be 0.12 W. Since FET's are excellent voltage-controlled RF switches with high gate-impedance requiring minimum control current or power, the overall PV-FET switch characteristics are superior to reported OE switches while requiring 10 to 100 times less optical power.

II. Device and Experiment

Fig. 1 depicts the PV-FET schematic with a depletion-mode FET. This PV-FET switched by illuminating the PV cell can be used as a series switch for reconfigurable antennas [4], [9]. The switch is on (closed) without illumination and the switch is off (open) with illumination to generate a photo-voltage exceeding the FET pinch-off voltage. The floating circuit illustrated in Fig. 1 is needed to obtain control voltage to the FET switch without connection to the electrical